Activating Bonds

van Zeist, W.

2011

document version
Publisher's PDF, also known as Version of record

8 Activation of C(sp^3)–X, C(sp^2)–X, and C(sp)–X bonds

Inspired by:
Willem-Jan van Zeist, F. Matthias Bickelhaupt
In Preparation

Abstract

We systematically investigate the activation of a series of variously hybridized bonds in simple model organic compounds by palladium. These comprise the C(sp^3)–X, C(sp^2)–X, and C(sp)–X bonds in X–substituted ethane, ethylene, and acetylene, respectively, with X = H, CH_3, and Cl. Although the bonds become stronger from sp^3 to sp hybridization, the activation barriers become lower. Our analysis show that the main reason for this is the increase in back-donation into the lower lying empty $\sigma^*_{C–X}$ LUMO orbital, and to a lesser extent, interactions with the $\pi_{C–C}$ and $\pi^*_{C–C}$ orbitals. A second effect is a decrease in steric repulsion as the substrate becomes smaller in going towards sp-hybridization. We include model ligand effects of the $PdCl^-$, $Pd(PH_3)_2$, and $Pd(PH_3)_2Cl^-$ catalytic compounds. We mainly focus on the effect the ligands have along the reaction path compared to the bare palladium, and in general see that the effect of the ligands on the interaction between catalyst and substrate becomes progressively stronger along the series of increased hybridization.

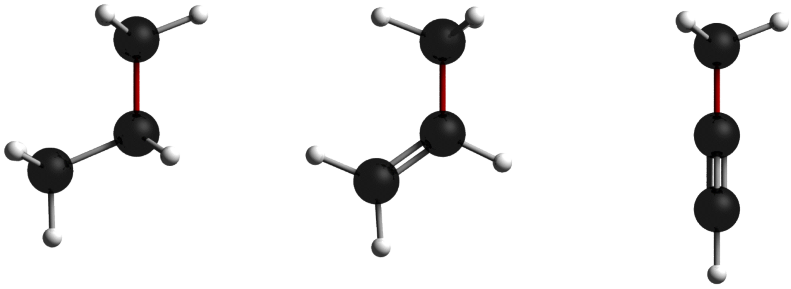

8.1 Introduction

The aim of this chapter is to investigate the influence of various hybridizations in simple model organic compounds. Specifically, we will look at the activation of C(sp^3)–X, C(sp^2)–X, and C(sp)–X bonds in X–substituted ethane, ethylene, and acetylene, respectively, with X = H, CH_3, and Cl (see Figure 8.1). The differently hybridized bonds give us an interesting range of bonds, when regarding the intrinsic bond strengths and bond properties connected to the hybridization. In this study we include the model phosphine and chloride anion ligands by using the catalysts $PdCl^-$, $Pd(PH_3)_2$, and $Pd(PH_3)_2Cl^-$.

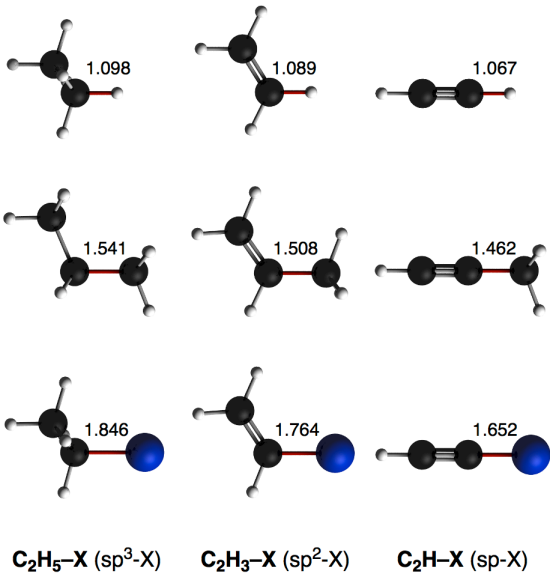

Figure 8.1 The substrates used in this chapter, including bond distances in Ångstrom.

The bond dissociation enthalpies (BDEs) and bond lengths of the substrates can be found in Table 8.1 (see also Figure 8.1). The strength of the bonds in general follow the increasing trend of sp^3 < sp^2 < sp. In all cases the range of bond strengths is around 30 kcal mol^{-1}, with for example C(sp^3)–H at 97.1 and C(sp)–H at 131.1 kcal mol^{-1}, with the trend being similar for X = H, CH_3, and Cl. Of course we see the well-known correlation between bond strengths and lengths, as the stronger bonds become shorter. As can be seen in Table 8.1, the ZORA-BLYP/TZ2P results (see section 2.2) compare well to experimentally determined values.

Table 8.1 Bond lengths (Å) and bond dissociation enthalpies at 298 K (in kcal mol^{-1}) of the substrates.

C–X	Bond Type	C–X (A)	BDE	BDE exp[a]
H_3CCH_2–H	sp^3–H	*1.098*	97.1	101.1
H_2CCH–H	sp^2–H	*1.089*	106.0	110.7
HCC–H	sp–H	*1.067*	131.1	133.3
H_3CCH_2–CH_3	sp^3–CH_3	*1.541*	79.8	89.0
H_2CCH–CH_3	sp^2–CH_3	*1.508*	92.3	101.4
HCC–CH_3	sp–CH_3	*1.462*	120.7	126.5
H_3CCH_2–Cl	sp^3–Cl	*1.846*	76.9	84.8
H_2CCH–Cl	sp^2–Cl	*1.764*	87.8	91.2
HCC–Cl	sp–Cl	*1.652*	106.2	-

[a] Experimental values taken from Blanksby and Ellison.[138]

Besides the bond strengths, obviously there are differences

between the hybridized bonds. Mainly of influence will be the σ^*_{C-X} LUMO anti-bonding and σ_{C-X} HOMO bonding orbital energies and the steric environment of the bond. The intrinsic bond orbital energies of the C–X bonds decrease along the hybridization series, which we can attribute to the increasing compactness and lower energy of the orbitals on the hybridized moiety along sp^3, sp^2, and sp. The decreasing σ^*_{C-X} LUMO orbitals indicate an intrinsically more stabilizing interaction with palladium, whose 4*d* orbitals donate into this orbital. The C(sp^3)–X bonds are the most sterically crowded, since the attacked carbon has four substituents in total, while C(sp)–X only has two. Therefore, the C(sp)–X type bonds are comparatively easy to approach. Both these factors will play a role, but are opposite to the effects of the trends in bond strengths.

8.2 Stationary points

The results of our calculations on reactions of uncoordinated palladium with these substrates are summarized in Table 8.2 (energies) and Figure 8.2 (geometries C–H activation), Figure 8.3 (C–C), and Figure 8.4 (C–Cl). In Table 8.2 the energies of the stationary points show the progress of the reaction. We have included the length of the activated C–X at each stationary point, which gives us insight into the progress of the reaction. The most important immediate observation is that the stronger bonds have lower insertion barriers, and thus decrease in the order of sp^3 > sp^2 > sp, see Table 8.2. This behavior can be explained by the aforementioned effects of increasing back-donation and decreasing steric crowding, which we will discuss in subsequent parts of this chapter. Previous studies have shown that the barrier heights for these model insertions increase from C–Cl to C–H to C–C (see chapter 3). Interestingly, in our systems, we see the same trend for each series of C–X (with the same hybridizations). This means that the different hybridizations do not change the selectivity of activation of the C–X bonds. As is also clear from Table 8.2, reactant complexes are considerably more stable (over -30 kcal mol^{-1}) for the unsaturated alkanes, due to strong inter-

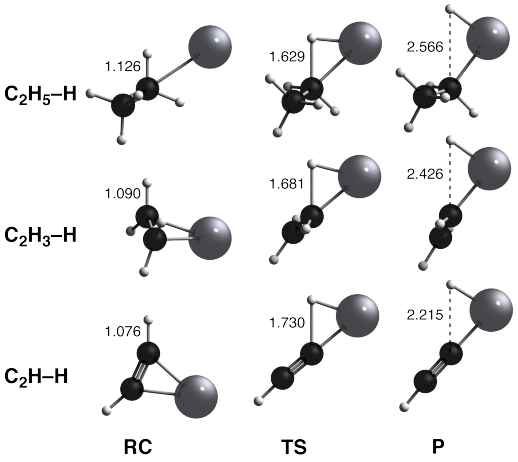

Figure 8.2 Geometries of the stationary points of the palladium insertion into the C–H bonds.

action with the π and π* orbitals. The changes in exothermicity are not as large as for the other stationary points, but still tend to follow the trends in barriers.

Table 8.2 Energies (kcal mol^{-1}) and C–X bond lengths (Å, in italics) of the stationary points of the bare palladium oxidative insertion reaction.

Pd	Bond Type	RC[a]		TS		P	
H_3CCH_2–H	sp^3–H	*1.126*	-6.8	*1.629*	4.4	*2.566*	-4.2
H_2CCH–H	sp^2–H	*1.090*	-33.8	*1.681*	-3.8	*2.426*	-7.9
HCC–H	sp–H	*1.076*	-33.7	*1.730*	-10.2	*2.215*	-11.6
H_3CCH_2–CH_3	sp^3–CH_3	*1.543*	-6.9	*1.974*	19.7	*3.095*	-8.7
H_2CCH–CH_3	sp^2–CH_3	*1.517*	-31.5	*1.995*	9.6	*2.991*	-8.9
HCC–CH_3	sp–CH_3	*1.479*	-31.9	*1.942*	6.3	*2.856*	-9.7
H_3CCH_2–Cl	sp^3–Cl	*1.890*	-13.6	*2.122*	-1.2	*2.270*	-33.0
H_2CCH–Cl	sp^2–Cl	*1.799*	-32.1	*2.089*	-16.3	*2.264*	-33.9
HCC–Cl	sp–Cl	*1.700*	-35.5	*1.922*	-17.9	*3.124*	-35.6

[a] Multiple closely related reactant complexes can in some cases be located; we only depict the one lowest in energy.

The geometries of the stationary points for the reactions with the different substrates are distinctly similar in appearance. All reactant complexes except for C(sp^3)–X show strong deformation due to the strong effects of both donation and back-donation upon complexation of the palladium. This is visible in Figure 8.2, Figure 8.3, and Figure 8.4, where the strong deformation of the substrate in the RCs is clearly seen. In these cases there is a slight elongation of the unsaturated C–C bonds by about 0.05 Å, indicating a slight weakening of the π-bond. This π-type interaction with the palladium first has to be broken during the course of the reaction, prior to the formation of the TS geometry. After this, although the interaction does not disappear completely, there is little influence from the π-type interactions; the differences in orbital interactions are mainly related to the back-donation into the LUMO σ^*_{C-X} orbital.

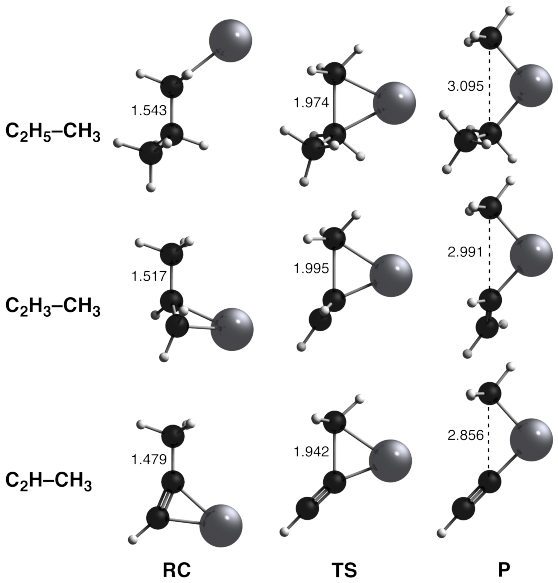

Figure 8.3 Geometries of the stationary points of the palladium insertion into the C–C bonds.

Looking in more detail at the energies of the stationary points, the insertion barrier of palladium into the C(sp^3)–H bond lies at 4.4 kcal mol^{-1}, directly proceeding from a slightly bound reactant complex at -6.8 kcal mol^{-1}. The reaction is exothermic as the product lies at -4.2 kcal mol^{-1} compared to the reactants. When moving to the unsaturated species, the barrier drops to -3.8 kcal mol^{-1} for C(sp^2)–H and -10.2 C for (sp)–H kcal mol^{-1}. The geometries show, in all transition states, a deformation of the substrate, both due to the stretching of the C–H bond, and the bending away of the substituent groups. The exothermicities of the reactions follow a similar trend, but the differences are somewhat smaller, ranging from -4.2 kcal mol^{-1} for the C(sp^3)–H to -11.6 for the C(sp)–H products.

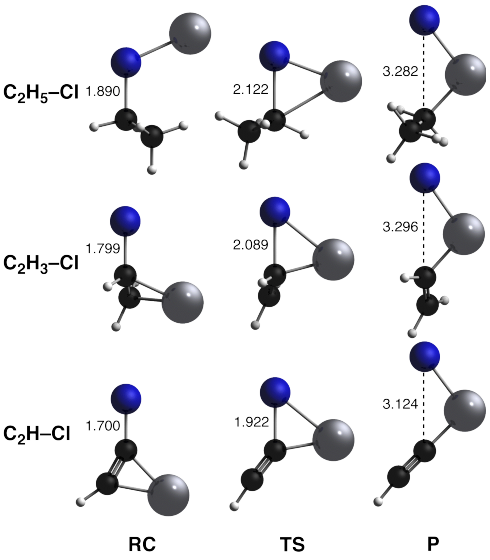

Figure 8.4 Geometries of the stationary points of the palladium insertion into the C–Cl bonds.

It is seen from the C–H bond lengths that the transition state shifts to the product-side of the reaction along sp^3, sp^2, and sp insertions, at increasing bond lengths. This trend is even more striking when taking into account that the trend in bond lengths in the substrates is actually reversed compared to that in the TSs. This is interesting since the barriers decrease along this series, yet the position of the TS indicates a strong influence of the increased destabilizing strain along the reaction path, which usually shifts the transition state towards the product side. We will treat this subject in more detail in the section covering the activation strain analysis of the entire reaction paths.

For the C–C insertions we find patterns in activation energies comparable to the C–H energies (but shifted upward by around 15 kcal mol^{-1}), as the barriers decrease along C(sp^3)–CH_3 (19.7), C(sp^2)–CH_3 (9.6), and C(sp)–CH_3 (6.3 kcal mol^{-1}). The exothermicity in principle follows a similar trend, but the differences are small as all the products lie within a 1 kcal mol^{-1} range around -9 kcal mol^{-1} relative to the reactants. The stabilities of the reactant complexes are very similar to those observed for the C–H insertions reactions.

For the C–Cl insertions we again see the same trend in activation energies (yet they are overall significantly lower due to the weaker C–Cl bond), with the TSs following the trend along C(sp^3)–Cl (-1.2), C(sp^2)–Cl (-16.3), and C(sp)–Cl (-17.9 kcal mol^{-1}). The exothermicity is far greater compared to the other series but still follows the same trend, with small differences: all the products lie within a range of 3 kcal mol^{-1} around -34 kcal mol^{-1} relative to the reactants.

8.3 Activation strain analysis

Figure 8.5 shows the potential energy surfaces (PESs) as obtained by IRC calculations, as well as the decomposition of the total energy into the strain and interaction parts. Of course the full energy paths correspond to the trends of energy barriers, but they also provide more information on the position of the TS on the reaction path. The strain energy behaves as one would expect and is higher for the stronger bonds, but the interaction energy becomes rapidly more stabilizing across the series of decreasing activation barrier. Note that strain energy is not only determined via the bond stretching, but also via a bending away of the substituent groups. Changes in interaction energy are easily the dominant factor, and outweigh the differences in bond strengths.

Noteworthy is the observation that the changes in interaction energy already take place at the beginning of the reaction path. Especially in the case of the C–H insertions, the differences in the interaction energy remain fairly steady as the reactions progress. In this case, the strain energies vary more strongly, and determine the shift of the TS towards the product side in going towards the C_2H–H activation. For the other bonds, the balance between strain and interaction and the behavior of the position of the transition state is more complex. In the insertions of C_2H_5–X, the palladium has a pronounced difficulty in reaching the bonds it activates, which translates into a weakening of the interaction energy already from early on in the reaction path. The interaction is strengthened when moving to the less sterically crowded unsaturated substrates (combined of course with the stronger interaction due to the lower lying LUMO orbital energy). This explains the relatively high barrier for the C_2H_5–X activation reactions. In all the cases for the unsaturated bonds, there is an initial destabilization of the interaction energy at the beginning of the reaction path, which is connected to the breaking away of the palladium from the stable reactant complex.

The general picture emerging from all the above analyses is that, in going from sp^3 to sp, back-donation increases due to lower σ^*_{C-X} LUMO orbitals on the substrates. Moreover, contrary to the case of the second period bonds (chapter 7), the donation

from the substrate into the 5*s* acceptor on palladium does not decrease, and remains fairly constant. This is on the one hand because of less dramatically changing σ HOMO orbitals compared to the substrates in chapter 7, and on the other hand because interaction with the π and π* orbitals add somewhat to stabilizing orbital interactions. At the same time, the repulsive interactions between substrate and palladium decrease substantially. Both effects lead to more stabilizing interaction energies.

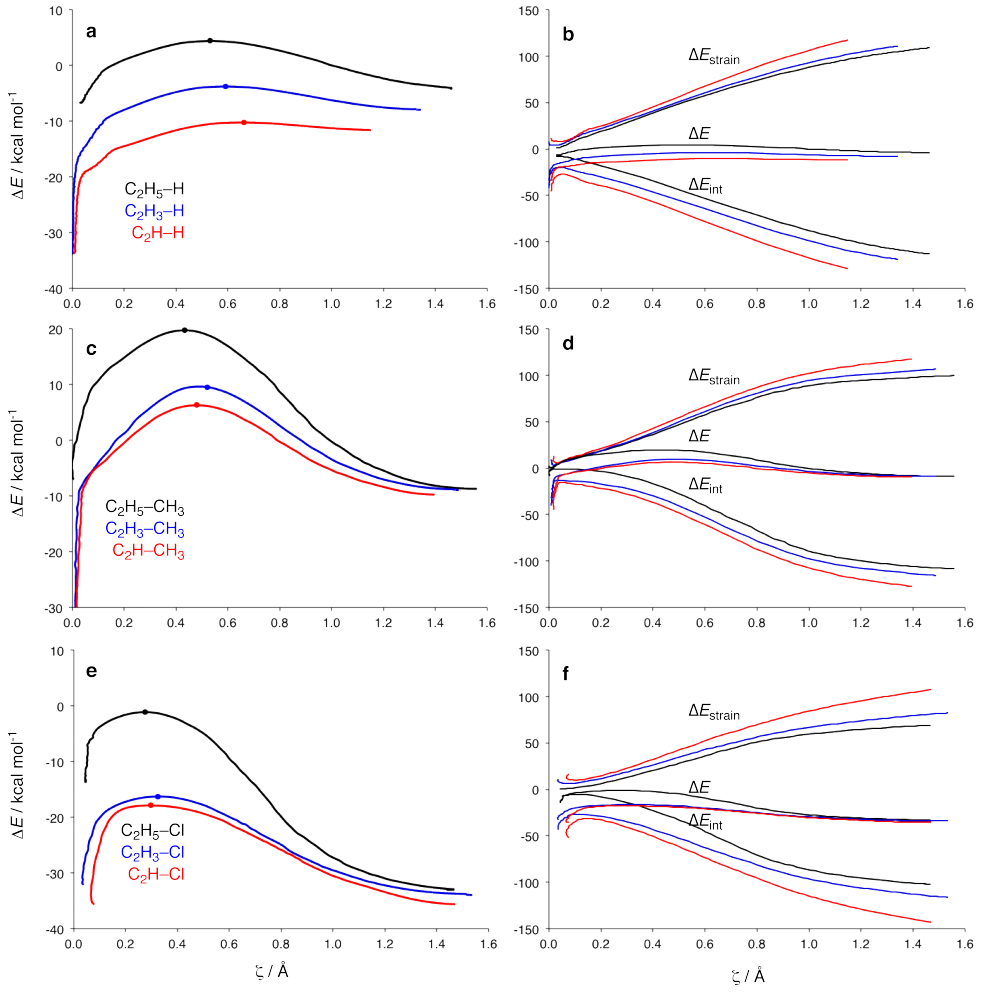

Figure 8.5 The potential energy surfaces (left) and activation strain analyses (right) for all palladium insertions. Transition states are indicated by dots in the potential energy surfaces.

To rigorously demonstrate these effects, we can construct a series of fictitious transition states with the C–Pd–X moiety as it is in the H_3CCH_2–X transition states. We then optimize each of the differently hybridized systems with this constraint, keeping

both the C–X distance and the distance of the palladium to the substrate fixed. Both are necessary, as at the actual TSs (but also along the entire reaction path) the changing interaction affects these geometrical variables quite substantially. These fictitious transition states give us more direct insight in the electronic and steric effect on a pure substitution of differently hybridized C–C moieties. The energy decomposition of the interaction energy of these geometries is shown in Table 8.3 (see also section 2.3). The results show very clearly the two major points that determine the interactions and thus barrier height. Firstly there is the increased orbital interaction because of decreased σ^*_{C-X} LUMO orbital energy, which is seen in the increasingly stabilizing ΔE_{oi} when going towards sp hybriziation. Upon closer inspection it can be seen that interactions with the π_{C-C} and π^*_{C-C} orbitals, although less important, also play a role in stabilizing ΔE_{oi}. The second important observation is a decreased ΔE_{Pauli} as the substrate becomes smaller in going moving from sp^3 to sp^2 or sp hybridization.

Table 8.3 Activation strain analysis of fictitious transition states (see text) of the Pd OxIn reactions.[a] All values are in kcal mol^{-1}.

	$\Delta E^{\ddagger}_{int}$	$\Delta E^{\ddagger}_{Pauli}$	$\Delta V^{\ddagger}_{elstat}$	$\Delta E^{\ddagger}_{oi}$
H_3CCH_2–H	-46.8	200.1	-159.6	-87.3
[H_2CCH][a]–H	-54.3	186.7	-148.4	-92.5
[HCC][a]–H	-66.5	156.0	-119.1	-103.4
H_3CCH_2–CH_3	-19.9	179.4	-128.0	-71.4
[H_2CCH][a]–CH_3	-30.0	166.0	-120.6	-75.4
[HCC][a]–CH_3	-40.6	154.8	-110.6	-84.7
H_3CCH_2–Cl	-12.2	115.2	-80.9	-46.6
[H_2CCH][a]–Cl	-23.0	105.9	-76.8	-52.1
[HCC][a]–Cl	-36.1	100.6	-69.8	-66.9

[a] All the C–Pd–X moieties constrained in the geometry of the C(sp^3)–X TS, the rest of the substrate was optimized.

8.4 Ligand effects

$Pd(PH_3)_2$: Table 8.4 shows the relative energies of the stationary values of the reactions of all types of bonds with the $Pd(PH_3)_2$ catalytic compound. Figure 8.6 shows the geometries and relevant geometrical data of the transition states for all reactions. As can be seen, $Pd(PH_3)_2$ as a catalyst destabilizes all the stationary points, for the saturated substrates the reactant complexes are almost non-existent. However, for the unsaturated substrates, a stable complex can be formed with palladium, despite the destabilizing effect of having to bend away the phosphine ligands to achieve this interaction. The destabilizing nature of adding the phosphine ligands was extensively discussed in chapter 3, and we here again see the substantial rise in transition state barriers. The general behavior across the different hybridizations remains similar, with the interaction energy being the dominant factor in determining the trends in activation barriers. The relative reactivity of the different bonds is not substantially influ-

enced and the differences in exothermicity are seen to be quite a bit larger, but still follow the same trends.

Table 8.4 Energies (kcal mol^{-1}) and C–X bond lengths (Å, in italics) of the stationary points of the $Pd(PH_3)_2$ oxidative insertion reaction.

$Pd(PH_3)_2$	Bond Type	RC[a]		TS		P	
H_3CCH_2–H	sp^3–H	*1.098*	-0.5	*1.728*	33.9	*2.421*	28.6
H_2CCH–H	sp^2–H	*1.090*	-9.5	*1.751*	25.4	*2.377*	22.5
HCC–H	sp–H	*1.076*	-11.1	*1.641*	13.8	*2.374*	9.7
H_3CCH_2–CH_3	sp^3–CH_3	*1.541*	-1.0	*2.143*	52.7	*2.861*	29.0
H_2CCH–CH_3	sp^2–CH_3	*1.520*	-6.1	*2.015*	42.5	*2.797*	26.7
HCC–CH_3	sp–CH_3	*1.462*	-8.2	*1.911*	38.5	*2.793*	18.1
H_3CCH_2–Cl	sp^3–Cl	*1.850*	-0.8	*2.358*	26.9	*3.177*	-8.3
H_2CCH–Cl	sp^2–Cl	*1.807*	-7.2	*2.099*	15.1	*3.127*	-10.6
HCC–Cl	sp–Cl	*1.654*	-14.0	*1.887*	12.3	*3.222*	-24.2

[a] Multiple reactant complexes can in some cases be located: we only depict the one lowest in energy.

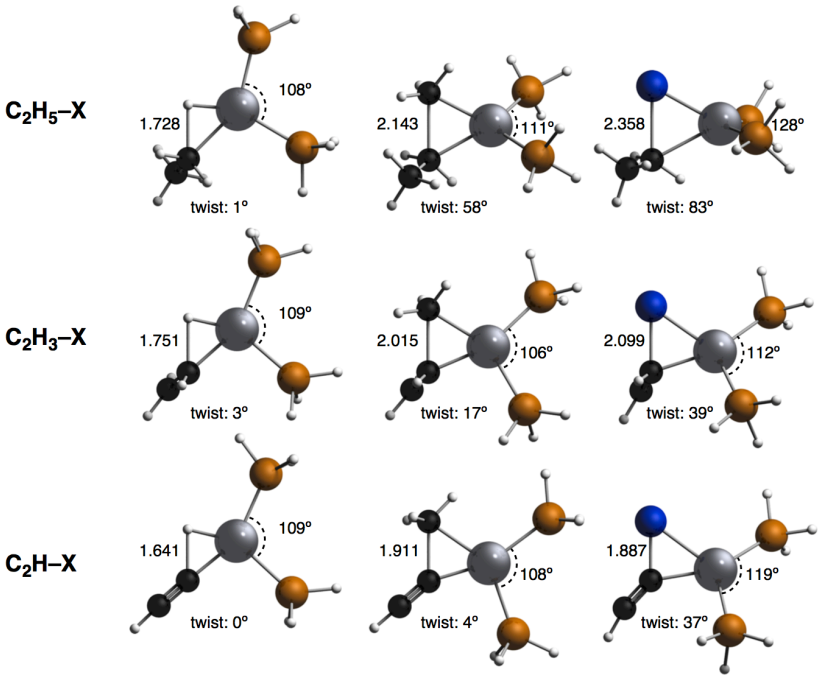

Figure 8.6 Geometries of the transition states of the insertion of $Pd(PH_3)_2$.

As can be seen from the geometries in Figure 8.6, all C–H insertion reactions are planar, as can be expected from the small repulsive interactions of the substrate. The bite angles do not differ much among the substrates and all lie around 109 degrees. For the C–C and C–Cl insertions, the transition states become more planar along the sp^3, sp^2 and sp insertion, as the steric congestion decreases with the smaller substrates. Bite

angle changes for these substrates are less pronounced, but depend heavily on the more flexible twist angle and the position of the transition state along the reaction coordinate. Overall there is again, as by now expected, a strong effect of steric influences on the geometry, in this case most visibly the twist angle, as the steric congestion decreases in going from sp^3 to sp^2 and sp hybridized substrates.

Along the reaction path (see Figure 8.7, similar analysis as shown in chapter 7) we can clearly see that the effect of adding the phosphine ligands is very similar for all substrates, but their destabilizing effect becomes gradually slightly smaller along sp^3, sp^2, and sp hybridization. It is seen that the strain energy changes little along the series. On the other hand, a small yet noticeable progressive increase in interaction across the series exists due to increased back-donation (which is more pronounced for the C(sp)–X substrate, where the interaction is already intrinsically stronger) and decreased steric repulsion between substrate and ligands. This effect is very similar to those described in earlier chapters. In Figure 8.7, it can also be more easily seen that, in going from sp^3 to sp, the difference between the Pd and $Pd(PH_3)_2$ potential energy surfaces changes due to a more steeply decreasing interaction, which shifts the position of the transition state to the left.

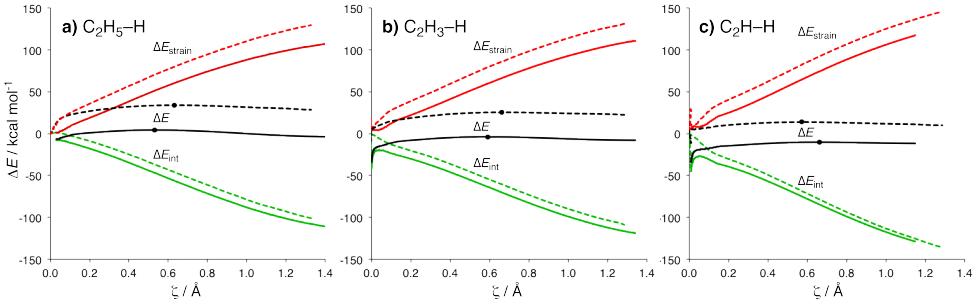

Figure 8.7 Comparison of the activation strain analysis of the oxidative insertions into the C–H bonds with bare palladium (solid lines) and with $Pd(PH_3)_2$ (dashed lines).

PdCl⁻: Table 8.5 shows the energies of all stationary points of the $PdCl^-$ insertion reactions. Figure 8.8 shows the geometries of the transition states of all reactions. The introduction of an anionic chloride ligand has, in concordance with previous research (see also the previous chapters), a strong stabilizing effect on all stationary points of the oxidative insertion reaction.[39] From Table 8.5 it is immediately obvious that the same trends as before are retained, yet the differences between the different substrates become larger. For example the barriers of the C–H insertions are found at -4.6 (sp^3), -16.9 (sp^2), and -32.5 kcal mol^{-1} (sp). The difference between sp^3 and sp insertions of

almost 30 kcal mol^{-1} is twice as large compared to the bare palladium paths (see Table 8.2). The trends in exothermicity also become stronger, yet still follow the same pattern.

Table 8.5 Energies (kcal mol^{-1}) and C–X bond lengths (Å, in italics) of the stationary points of the $PdCl^-$ oxidative insertion reaction.

$PdCl^-$	Bond Type	RC[a]		TS		P	
H_3CCH_2–H	sp^3–H	*1.136*	-12.5	*1.606*	-4.6	*2.221*	-8.2
H_2CCH–H	sp^2–H	*1.092*	-40.9	*1.686*	-16.9	*2.111*	-17.7
HCC–H	sp–H	*1.079*	-42.2	*1.593*	-32.5	*2.218*	-34.2
H_3CCH_2–CH_3	sp^3–CH_3	*1.540*	-12.8	*1.908*	16.6	*2.815*	-8.9
H_2CCH–CH_3	sp^2–CH_3	*1.523*	-38.2	*1.915*	1.1	*2.797*	-13.8
HCC–CH_3	sp–CH_3	*1.485*	-38.8	*1.843*	-7.8	*2.788*	-26.8
H_3CCH_2–Cl	sp^3–Cl	*1.952*	-17.2	*2.254*	-6.9	*3.247*	-53.6
H_2CCH–Cl	sp^2–Cl	*1.871*	-45.9	*2.196*	-25.0	*3.185*	-55.9
HCC–Cl	sp–Cl	*1.758*	-50.2	*1.984*	-30.2	*3.189*	-66.4

[a] Multiple closely related reactant complexes can in some cases be located: we only depict the one lowest in energy.

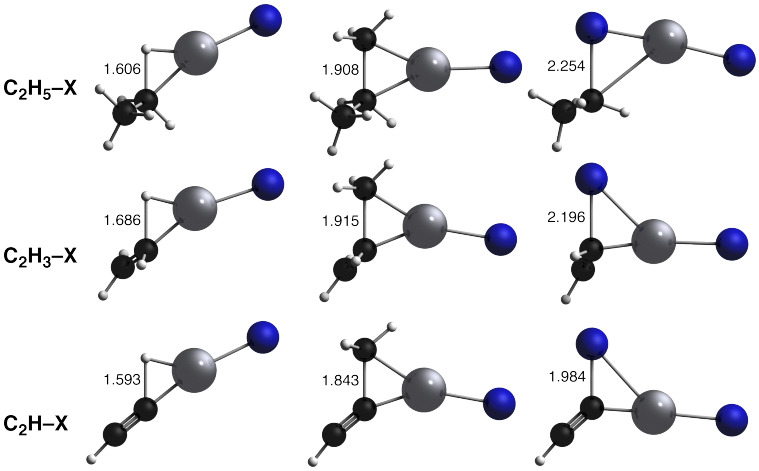

Figure 8.8 Geometries of the transition states of the insertion of $PdCl^-$.

When looking at the C–X bond lengths in Figure 8.8 we see that, especially in the case of C_2H–H and C_2H-CH_3, the point of the TS is much closer to the reactant side at a shorter bond stretch compared to the bare palladium reaction paths. This is in line with the idea of extra stabilization of the already strong interaction for these bonds when the chloride anion is present. All this indicates that again, an increase in interaction has a stronger effect when the interaction is already inherently strong.

The effects of an increased stabilization are clearly seen along the reaction coordinate when comparing the Pd and $PdCl^-$ paths for the C–H hybridization series (see Figure 8.9). In Figure 8.9a, the stabilizing effect of the anion is already unmistakable in

the reaction path of the C_2H_5–H insertion. Especially when going towards the C_2H–H insertion, it is clear that the effect of the increased destabilization is much stronger across the series, and also shifts the transition state towards the left.

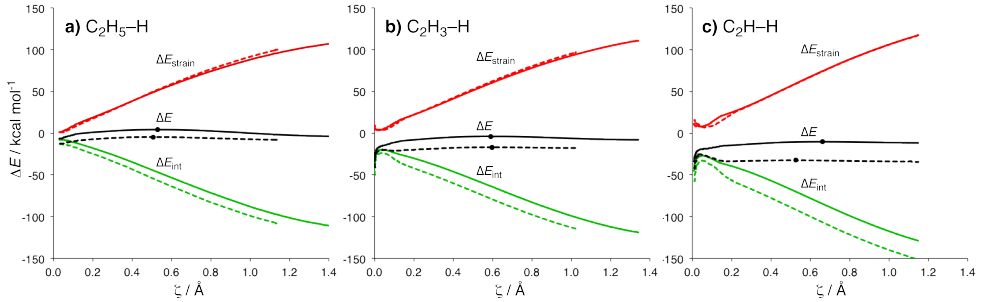

Figure 8.9 Comparison of the activation strain analysis of the oxidative insertions with bare palladium (solid lines) and with $PdCl^-$ (dashed lines). Graphs b and c can be seen to contain a second low-barrier transition state at the start of the $PdCl^-$ insertion reaction path. This TS leads from the π-complex (RC) to a structure where the $PdCl^-$ is bound the C–H bond, from which point the OxIn continues.

$Pd(PH_3)_2Cl^-$: As in the previous chapters, we have also incorporated the phosphine catalyst, including the influence of the anionic chloride ligand (see Figure 8.10 and Table 8.6). The reactant complexes for the $C(sp^3)$–X substrates are again, like $Pd(PH_3)_2$, essentially unbound. Also similar are the RCs for the unsaturated substrates, where the catalyst moiety retains the geometry with the Cl^- acting as a chelating 'backbone' for the two phosphines. Also, for C_2H_5–X the transition states are somewhat destabilized compared to the $Pd(PH_3)_2$ transition states, as was also noted in the previous chapters, due to the higher strain as the chloride anion has to break free from the palladium and migrate to its position on the phosphine ligands. However, when we continue along C_2H_3–X and C_2H–X, we see that there is a clear increased stabilization of the TS compared to $Pd(PH_3)_2$, while at the same time there is a clear trend of decreasing C–X bond distances in the TS. Both of these observations point towards what we have already observed in the previous chapters: the chloride anion actually increases the back-donation due to the presence of the negative charge. This increase is more notable in the $C(sp^2)$–X and especially C(sp)–X reactions, as the interaction is intrinsically strong for these substrates.

Table 8.6 Energies (kcal mol^{-1}) and C–X bond lengths (Å) of the stationary points of the $Pd(PH_3)_2Cl^-$ oxidative insertion reaction.

$Pd(PH_3)_2Cl^-$	Bond Type	RC[a]		TS		P	
H_3CCH_2–H	sp^3–H	*1.098*	-1.7	*1.669*	35.7	*2.550*	25.3
H_2CCH–H	sp^2–H	*1.090*	-7.0	*1.637*	23.9	*2.452*	17.9
HCC–H	sp–H	*1.080*	-10.0	*1.492*	9.4	*2.457*	1.3
H_3CCH_2–CH_3	sp^3–CH_3	*1.541*	-1.7	*2.065*	57.7	*2.893*	25.1
H_2CCH–CH_3	sp^2–CH_3	*1.524*	-7.0	*1.954*	43.0	*2.833*	21.7
HCC–CH_3	sp–CH_3	*1.489*	-10.0	*1.868*	37.2	*2.858*	9.7
H_3CCH_2–Cl	sp^3–Cl	*1.877*	-0.4	*2.253*	29.9	*3.233*	-18.5
H_2CCH–Cl	sp^2–Cl	*1.839*	-8.4	*2.093*	12.6	*3.178*	-22.1
HCC–Cl	sp–Cl	*1.766*	-17.5	*1.869*	8.3	*3.284*	-39.8

[a] Multiple closely related reactant complexes can in some cases be located: we only depict the one lowest in energy.

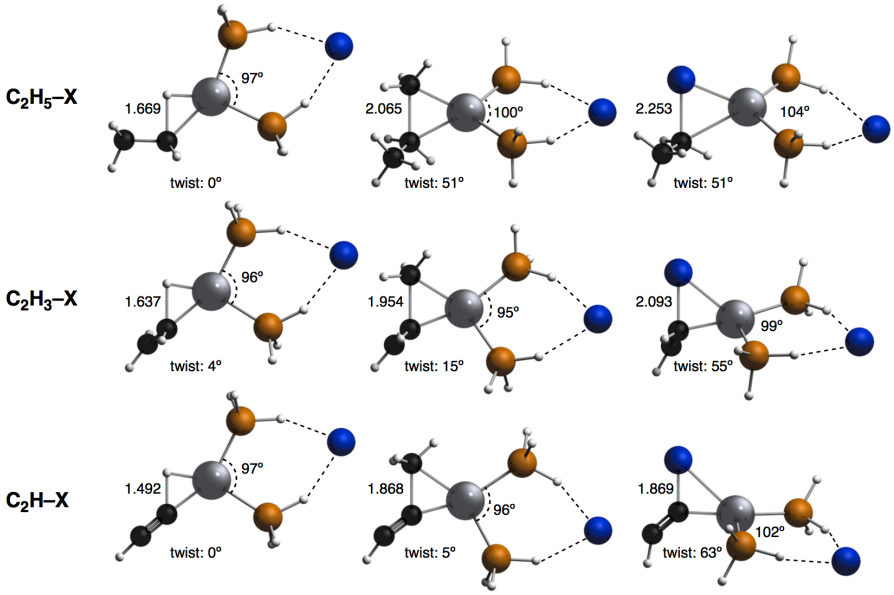

Figure 8.10 Geometries of the transition states of the insertion of $Pd(PH_3)_2Cl^-$.

Again we can compare the reaction paths of the insertion of $Pd(PH_3)_2Cl^-$ into C–H bonds with the reaction of bare palladium (see Figure 8.11). For the comparison we used the TV-IRC approach to construct partial, but still useful, potential energy surfaces (see section 2.7). In Figure 8.11a we again see what was also the case for $Pd(PH_3)_2$, a slight destabilization of the interaction combined with a strong increase of the destabilizing strain energy. However, since the back-donation process is enhanced due to the Cl^-, the interaction curve becomes actually more stabilizing compared to bare Pd when arriving at the C_2H–H insertion process. It is also clear that the interaction curve becomes steeper and the point of the transition state is shifted to the left.

This very clearly shows the main reason for the comparatively low barriers for the more unsaturated substrates. Also it explains the somewhat larger differences between the C(sp^3)–X and C(sp)–X for the $Pd(PH_3)_2Cl^-$ insertion, compared to that without the anionic assistance.

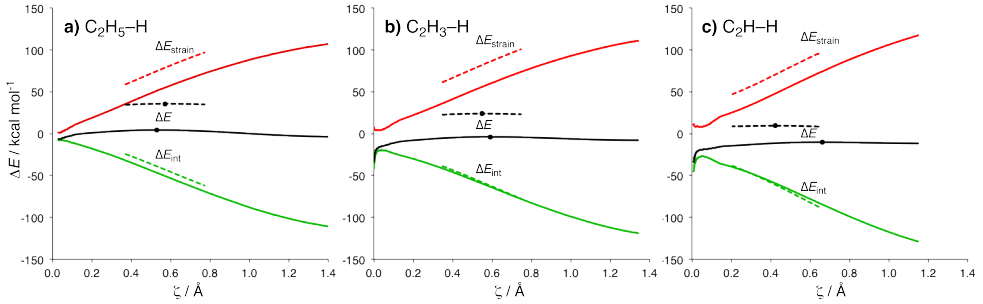

Figure 8.11 Comparison of the activation strain analysis of the oxidative insertions into the C–H bonds with bare palladium (solid lines) and with $Pd(PH_3)_2Cl^-$ (dashed lines, TV-IRC).

8.5 Conclusions

We have investigated the activation of C(sp^3)–X, C(sp^2)–X, and C(sp)–X bonds in X–substituted ethane, ethylene, and acetylene, respectively, with X = H, CH_3, and Cl. We observe a steady decrease in barrier heights of their oxidative addition, despite the fact that the bonds become stronger along the series. There are two important reasons for this behavior: 1) in going from sp^3 to sp hybridization, back-donation is increased due to lower lying σ* LUMO orbitals on the substrate, and to a lesser extent, due to interactions with the π_{C-C} and π^*_{C-C} orbitals; 2) decreased steric repulsion as the substrate becomes smaller in going towards sp-hybridization. Moreover, contrary to the case of the second period bonds (chapter 7), the donation from the substrate into the 5*s* acceptor on palladium does not decrease, and remains fairly constant. The latter explains why (compared to the second period bonds) the interaction is strong enough to overcome the opposing trend of destabilizing strain due to the trends in bond strengths.

It was shown, as in the previous chapter, to be highly informative to compare the ligand effects directly with the reaction paths of the bare palladium. It then becomes clear that, in all cases, the interaction with the substrate usually becomes progressively stronger along the series of hybridization (after initial stabilization or destabilization on the saturated substrate). This results in a general tendency of the downward trends in activation barriers to be enhanced. This conclusion has of course some similarities to that described in chapter 7.